# We are IntechOpen, the world's leading publisher of Open Access books Built by scientists, for scientists

**4,800**
Open access books available

**122,000**
International authors and editors

**135M**
Downloads

Our authors are among the

**154**
Countries delivered to

**TOP 1%**
most cited scientists

**12.2%**
Contributors from top 500 universities

CLARIVATE ANALYTICS BOOK CITATION INDEX INDEXED

WEB OF SCIENCE™

Selection of our books indexed in the Book Citation Index in Web of Science™ Core Collection (BKCI)

## Interested in publishing with us?
## Contact book.department@intechopen.com

Numbers displayed above are based on latest data collected.
For more information visit www.intechopen.com

26

# Pattern recognition methods for improvement of differential protection in power transformers

Abouzar Rahmati
*University Of Ilam*
*Iran*

## 1. Introduction

Differential protection was already applied towards the end of the 19th century, and was one of the first protection systems ever used.
Faults are detected by comparison of the currents flowing into and out of the protected plant item. As a result of the fast tripping with absolute selectivity it is suited as main protection of all important items of plant, i.e. generators, transformers, busbars as well as cables and overhead lines and feeders at all voltage levels.
The power transformer protection is of critical importance in power systems. Since minimization of frequency and duration of unwanted outages is very desirable there is a high demand imposed on power transformer protective relays. This includes the requirements of dependability associated with no mal-operations, security associated with no false tripping, and operating speed associated with short fault clearing time.
One of the main concerns in differential protection of this particular component of power systems lies in the accurate and rapid discrimination of magnetizing inrush current from different internal faults currents. This is because the magnetizing inrush current, which occurs during the energizing the transformer, generally results in several times full load current and therefore can cause mal-operation of the relays. Such mal-operation of differential relays can affect both the reliability and stability of the whole power system.
The principle of differential protection is initially described in this chapter. Subsequently different protection schemes are covered in the next sections. At last an algorithm based on pattern recognition of current signals using wavelet transform which is a power signal processing tool is proposed.

## 2. Mode of operation of differential protection

The differential protection is 100% selective and therefore only responds to faults within its protected zone. The boundary of the protected one is uniquely defined by the location of the current transformers. Due to simple current comparison, the principle of differential protection is very straight forward.

Generators, motors and transformers are often protected by differential protection, as the high sensitivity and fast operation is ideally suited to minimize damage. On feeders the differential protection is mainly used to protect cables, particularly on short distances where distance protection cannot be readily applied.
The prime objective of busbar differential protection is fast, zone selective clearance of busbar faults to prevent large system outages and to ensure system stability. Mal-operation must be avoided at all cost as these could result in extensive supply interruption.

## 3. Principles of differential protection

The basic principles which have been known for decades are still applicable and independent of the specific device technology.
The differential protection compares the measured values of signals with regard to magnitude and phase. This is possible by direct comparison of instantaneous values or by vector (phasor) comparison. In each case the measurement is based on Kirchhoff's laws which state that the geometric (vector) sum of the currents entering or leaving a node must add up to 0 at any point in time. The convention used in this context states that the currents flowing into the protected zone are positive, while the currents leaving the protected zone are negative. The current differential protection is the simplest and most frequently applied form of differential protection. The measuring principle is shown in Fig. 1. X is the winding of the protected machine. The relay compares an operating current with a restraining current. The operating current (also called differential current), $I_O$, and the restraining current, $I_R$, are obtained as below:

$$I_O = |I_1 + I_2| \qquad (1)$$
$$I_R = K|I_1 - I_2|$$

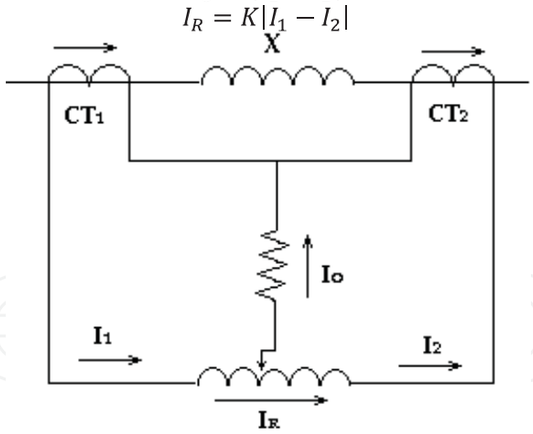


Fig. 1. Differential relay connection diagram

When there is no internal fault, the current entering in X is equal in phase and magnitude to current leaving X. The CT's are of such a ratio that during the normal conditions or for external faults (Trough faults) the secondary currents of CT's are equal. The relay generates a tripping signal if the operating current, $I_O$, is greater than a percentage of the restraining current, $I_R$,, according to:

$$I_O > KI_R + I_P \tag{2}$$

where K is the relay operating characteristic, that consists of a straight line having a slope equal to K. Intersection of this characteristic with vertical axis ($I_O$) define the relay minimum pickup current, $I_P$. The relay percentage restraint characteristic typically has an excellent behavior, but it has problems discriminating fault currents from false differential currents caused by magnetizing inrush and transformer over excitation.

## 4. Main difficult in differential protection

Differential protection is established as the main protection for transformer due to its simple principle of operation and sensitivity. However, a key problem of differential protection is accurate and rapid discrimination of magnetizing inrush current from an internal fault current.

Initial magnetizing due to switching a transformer in is considered the most severe case of an inrush. When a transformer is de-energized (switched-off), the magnetizing voltage is taken away, the magnetizing current goes to zero while the flux follows the hysteresis loop of the core. This results in certain remanent flux left in the core. When, afterwards, the transformer is re-energized by an alternating sinusoidal voltage, the flux becomes also sinusoidal but biased by the remanence. The residual flux may be as high as 80-90% of the rated flux, and therefore, it may shift the flux-current trajectories far above the knee-point of the characteristic resulting in both large peak values and heavy distortions of the magnetizing current.

Figure 2 shows a typical inrush current. The waveform displays a large and long lasting dc component, is rich in harmonics, assumes large peak values at the beginning (up to 30 times the rated value), decays substantially after a few tenths of a second, but its full decay occurs only after several seconds (to the normal excitation level of 1-2% of the rated current).

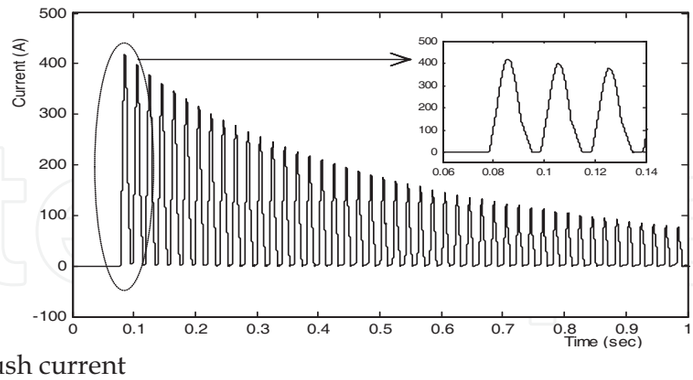


Fig. 2. Typical inrush current

It is evident that relaying protection should be initiated in response to internal fault but not to inrush current. To avoid the needless trip by magnetizing inrush current, many different restrain methods are proposed in recent years.

Since the magnetizing branch representing the core appears as a shunt element in the transformer equivalent circuit, the magnetizing current upsets the balance between the currents at the transformer terminals, and is therefore experienced by the differential relay

as a "false" differential current. The relay, however, must remain stable during inrush conditions. In addition, from the standpoint of the transformer life-time, tripping-out during inrush conditions is a very undesirable situation (breaking a current of a pure inductive nature generates high overvoltage that may jeopardize the insulation of a transformer and be an indirect cause of an internal fault).

## 5. The proposed schemes for differential protection

### 5.1 Recognition of type of signals using Fourier Transform

Magnetizing inrush current generally contains a large second harmonic component in comparison to an internal fault. As a result conventional transformer protection systems are designed to block during inrush transients by this large second harmonic. The ratio of the second harmonic of differential current in excess of a preset threshold is interpreted as a present of magnetizing inrush.

Let us calculate the harmonic component of a typical inrush current waveform. We will assume a simplified waveform for the inrush current. Let the magnetizing characteristic be a vertical line in the $\emptyset - i$ plane, and be a straight line with a finite slope in the saturated region. This makes the current waveform of Figure 3 acquire the shape shown in Figure 4.

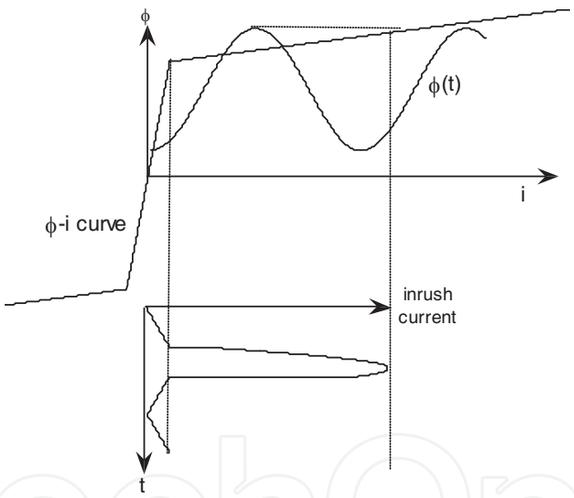


Fig. 3. Magnetizing current during energizing of a transformer

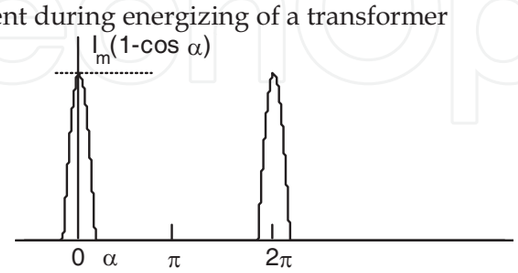


Fig. 4. Idealized inrush current waveform

The flux in the core is above the saturation knee point for a total angular span of $2 \propto$ radians, and the corresponding current is a portion of a sine wave. For the remainder of the

period, the current is zero. Although this is an approximation, it is quite close to an actual magnetizing current waveform. We may use Fourier series analysis to calculate the harmonics of this current. Consider the origin to be at the center of a current pulse, as shown in Figure 4. Then, the approximation for the current waveform is:

$$i(\theta) = \begin{cases} I_m(\cos\theta - \cos\alpha) & 0 \le \theta \le \alpha \ , \ (2\pi - \alpha) \le \theta \le 2\pi \\ 0 & \alpha \le \theta \le (2\pi - \alpha) \end{cases} \tag{3}$$

Since this choice of the origin gives a symmetric waveform about $\theta = 0$, we may use the cosine Fourier series for the current. The n$^{th}$ harmonic is given by:

$$a_n = \frac{1}{\pi}\int_0^{2\pi} i(\theta)\cos(n\theta)\, d\theta = \frac{2}{\pi}\int_0^{\alpha} I_m\,(\cos\theta\cos n\theta - cos\alpha\cos n\theta)\, d\theta$$
$$= \frac{I_m}{\pi}\left[\frac{1}{n+1}\sin(n+1)\alpha + \frac{1}{n-1}\sin(n-1)\,\alpha - \frac{2}{n}\cos\alpha\sin n\alpha\right] \tag{4}$$

The peak of the current wave is $I_m(1-\cos\alpha)$, and the fundamental frequency component $a_1$ is given by:

$$a_1 = \frac{I_m}{\pi}\left[\alpha - \frac{1}{2}\sin 2\alpha\right] \tag{5}$$

The relative magnitude of various harmonic components with respect to the fundamental frequency component, as calculated from equation (4) and (5), is tabulated in Table 1 up to the 13$^{th}$ harmonic, and for saturation angles of $60^{\circ}, 90^{\circ}$ and $120^{\circ}$. It should be noted that when the saturation angle is $90^{\circ}$ there are no odd harmonics present. As the angle of saturation increases, the harmonic content decreases: indeed, if $\alpha$ becomes $\pi$ there will be no harmonics at all. However, in most cases, $\alpha$ is much less than $\pi$, and a significant amount of harmonics are present in the magnetizing inrush current. Of all the harmonic components, the second is by far the strongest.

| Harmonic | $a_n/a_1$ | | |
|---|---|---|---|
| | $\alpha = 60^{\circ}$ | $\alpha = 90^{\circ}$ | $\alpha = 120^{\circ}$ |
| 2 | 0.705 | 0.424 | 0.171 |
| 3 | 0.352 | 0.000 | 0.086 |
| 4 | 0.070 | 0.085 | 0.017 |
| 5 | 0.070 | 0.000 | 0.017 |
| 6 | 0.080 | 0.036 | 0.019 |
| 7 | 0.025 | 0.000 | 0.006 |
| 8 | 0.025 | 0.029 | 0.006 |
| 9 | 0.035 | 0.000 | 0.008 |
| 10 | 0.013 | 0.013 | 0.003 |
| 11 | 0.013 | 0.000 | 0.003 |
| 12 | 0.020 | 0.009 | 0.005 |
| 13 | 0.008 | 0.000 | 0.002 |

Table 1. Harmonics of the magnetizing inrush current

Magnetizing inrush current generally contains a large second harmonic component in comparison to an internal fault. As a result conventional transformer protection systems are

designed to block during inrush transients by this large second harmonic. The ratio of the second harmonic of differential current in excess of a preset threshold is interpreted as a present of magnetizing inrush. However, the second harmonic due to CT saturation component may also be generated during internal faults. Moreover, it was found that in certain cases, the second harmonic generated during internal faults in transformers is relatively large, which impairs the ability of this kind of the criterion. Consequently, the commonly used conventional differential protection technique based on the second harmonic restraint will thus have difficulty in distinguishing between internal fault currents and inrush currents.

### 5.2 Wave shape recognition of signals in time domain

Wave shape recognition techniques represent another alternative for discriminating internal faults from inrush current signals. In this kind inrush restraining methods pays attention to the periods of low and peaks values of the inrush current signal in the time domain.

It has been observed from Fig. 2 that the inrush wave is distinguished from a fault wave (which is sinusoidal wave shape) by a period in each cycle during which very low magnetizing currents (i.e. the normal exciting currents) flow, when the core is not in saturation. This property of the inrush current can be used to distinguish this condition from an internal fault. The condition to declare inrush would be that during a power system frequency cycle, there should always be an interval of time when an instantaneous differential current is equal to the normal magnetizing current, which is close to zero (below 0.5 %). This interval must be at least about 1/4 of the period, that is, about 5 ms in 50 Hz power systems.

Generally, there are basically two inrush restraining methods of wave shape recognition:

The first, and more common approach, pays attention to the periods of low and flat values in the inrush current ("dwell-time" — criterion 1), and the second algorithm pays attention to the sign of the peak values and the decaying rate of the inrush current (criterion 2).

A. Criterion 1

The hypothesis of magnetizing inrush may be ruled out if the differential current does not show in its every cycle a period lasting no less than 1/4 of a cycle in which the shape of the waveform is both flat and close to zero (see Figure 5).

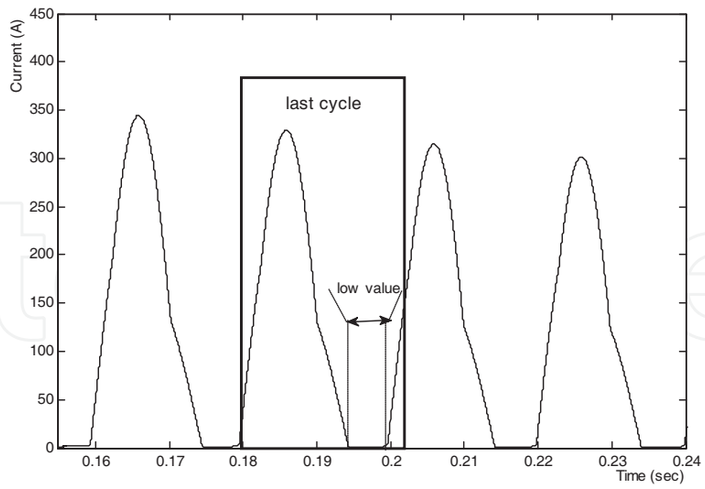


Fig. 5. Illustration of the direct waveform recognition of inrush (criterion 1)

This form of direct waveform restraining regardless of its implementation shows weaknesses:

(a) the recognition of an internal fault versus magnetizing inrush takes one full cycle

(b) the CTs, when saturated during inrush conditions (very likely due to the dc component in the current), change the shape of the waveform within the dwell periods (Figure 6) and may cause a false tripping

(c) during severe internal faults, when the CTs saturate, their secondary currents may also show periods of low and flat values exposing the relay to missing operations

B. Criterion 2

The hypothesis of magnetizing inrush may be ruled out if the differential current has its peaks displaced by half a cycle, and any two consecutive peaks are not of the same polarity (see Figure 6). This method needs robust detection of the peak values. Timing between two consecutive peaks must be checked with some tolerance margin accounting for the frequency deviations.

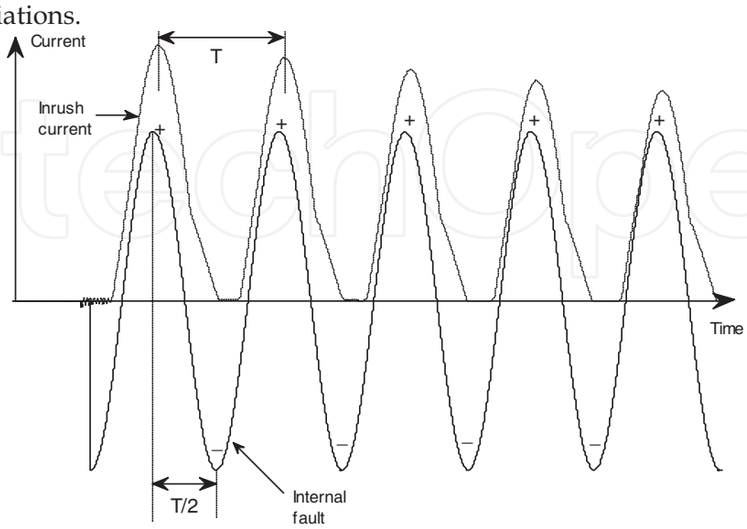


Fig. 6. Illustration of internal fault and magnetizing inrush currents (criterion 2)

Theoretically, this method needs three quarters of a cycle to distinguish between internal faults and inrush conditions. The first peak of the fault current appears after a quarter of a cycle, the next one - half a cycle later. With the second peak arriving, the criterion rejects the inrush hypothesis and sets the tripping permit.
The main disadvantage of this algorithm is the need of cross polarization between the phases. Not always all three phases show the typical inrush uni-polar waveform. Also, during very smooth energization of a protected transformer (what may accidentally happen owing to the adequate relation between the switching angle and the remanent flux), this criterion will fail.
This criterion may be also used in its indirect form as a modifier for the instantaneous differential overcurrent element. Defining the overcurrent principle as:

$$TRIP = |i_D| > \delta \tag{6}$$

and specifying one threshold, one needs to adjust this threshold very high to prevent false trippings (above the highest inrush current). One may, however, re-define the operating principle (Figure 7):

$$TRIP = (i_D > \delta_+) \;\&\; (i_D < \delta\_) \tag{7}$$

and use two thresholds to detect the uni-polarity/bi-polarity of the signal (Figure 7). When using the modified overcurrent principle, the setting may be adjusted as low as one third of the traditional threshold. This allows much more internal faults to be quickly detected by the unrestrained overcurrent algorithm.

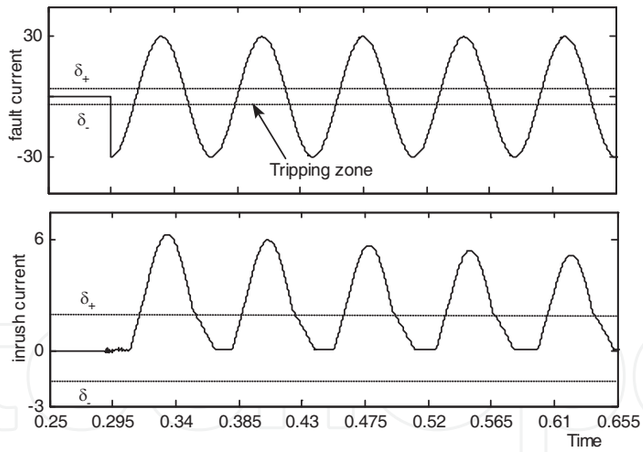


Fig. 7. Illustration of the double-threshold overcurrent principle

### 5.3 Mathematical morphology for recognition of signals

Mathematical morphology (MM) is a relatively new tool for image and signal processing. It is based on theoretic set concept, extracting object features by choosing a suitable structuring shape as a probe. Morphological operations, based on set transformation, are used to convert an image or signal into a quantitative description of its geometrical structure. The applications of MM are mainly focused on image processing, nonlinear filtering, machine vision, and pattern recognition.

Some schemes are proposed to identify inrush current signals from other conditions by using a morphological decomposition scheme (MDS) based on the morphological wavelet. In these approaches differential currents decompose into a series of components by designed morphological operators; then the extracted features of these components will employ for inrush signals identification.

MM is a nonlinear approach and has been widely used in many signal/image processing applications due to its simple and robust performance. Dilation and erosion are the two basic operators of MM, which are defined as

$$(f \oplus b)(x) = max\{f(x-s) + b(s)\}, x \in D_f, s \in D_b \quad (8)$$

$$(f \ominus b)(x) = min\{f(x+s) - b(s)\}, x \in D_f, s \in D_b \quad (9)$$

Where $f$ is the signal under processing, $b$ is the $SE$, and $D_f$ and $D_b$ represent the field of definition of $f$ and $b$, respectively.

The morphological wavelet is a nonlinear multiresolution signal decomposition scheme. A formal definition of the morphological wavelet is presented as follows. Assume that sets $V_j$ and $W_j$ exist. $V_j$ is referred to as the signal space at level $j$, and $W_j$ is the detail space at level $j$. The morphological wavelet has two analysis operators which together decompose a signal in the direction of increasing $j$. The signal-analysis operator $\psi_j^{\uparrow}$ maps a signal from $V_j$ to $V_{j+1}$ (i.e., $\psi_j^{\uparrow} : V_j \longrightarrow V_{j+1}$), while the detail analysis operator maps it from $V_j$ to $W_{j+1}$ (i.e., $\omega_j^{\uparrow} : V_j \longrightarrow W_{j+1}$). On the other hand, a synthesis operator proceeds in the direction of decreasing $j$, denoted as $\Psi_j^{\downarrow} : V_{j+1} \times W_{j+1} \longrightarrow V_j$.

In order to yield a complete signal representation, the mappings $(\psi_j^{\uparrow}, \omega_j^{\uparrow})$ and $\Psi_j^{\downarrow}$ should be inverses of each other, i.e.,

$$\begin{cases} \Psi_j^{\downarrow}\left(\psi_j^{\uparrow}(x_j), \omega_j^{\uparrow}(x_j)\right) = x_j \\ \psi_j^{\uparrow}\left(\Psi_j^{\downarrow}(x_{j+1}, y_{j+1})\right) = x_{j+1} \\ \omega_j^{\uparrow}\left(\Psi_j^{\downarrow}(x_{j+1}, y_{j+1})\right) = y_{j+1} \end{cases} \quad (10)$$

Here, $x$ is called the approximation signal and $y$ is the detail signal. Therefore, decomposing an input signal $x_0 \in V_0$ with the following recursive analysis scheme is:

$$x_0 \longrightarrow \{x_1, y_1\} \longrightarrow \{x_2, y_2, y_1\} \longrightarrow \cdots \longrightarrow \{x_j, y_j, y_{j-1}, \ldots, y_1\} \longrightarrow \cdots$$

Where $x_{j+1} = \psi_j^{\uparrow}(x_j)$, $y_{j+1} = \omega_j^{\uparrow}(x_j)$, and $x_0$ can be exactly reconstructed from $x_j$ and $y_j, y_{j-1}, \ldots, y_1$ by means of the following recursive synthesis scheme:

$$x_{j-1} = \Psi_{j-1}^{\downarrow}(x_j, y_j) \quad (11)$$

Let us analyse the scheme in detail which was proposed (Z. Lu et al, 2009) based on morphological decomposition scheme. This work proposes MDS based on the concepts of morphological wavelet. The operators in the scheme are specifically designed by using fundamental morphological operators-dilation and erosion-and are able to decompose

differential currents signals into a series of components for the purpose of inrush identification.

In MDS, the analysis operators $\psi_j^{\uparrow}$ and $\omega_j^{\uparrow}$ and the synthesis operator $\Psi_j^{\downarrow}$ are defined as

$$\begin{aligned} \psi_j^{\uparrow}(r_j) &= r_{j+1} = \gamma(r_j) \\ \omega_j^{\uparrow}(r_j) &= s_{j+1} = r_j - \gamma(r_j) \\ \Psi_j^{\downarrow}\left(\psi_j^{\uparrow}(r_j)\ \omega_j^{\uparrow}(r_j)\right) &= r_j = r_{j+1} + s_{j+1} \end{aligned} \tag{12}$$

Where $r_1 = I$ is the transformer differential current. $s_1 = \emptyset$ and $j = 1,2,\ldots$. With the analysis operators, the signal $I$ is decomposed into a set of components $\{s_2, \ldots, s_j, r_j\}$; and by the synthesis operator, it can be reconstructed from $I = r_j + \sum_j s_j$. $\gamma(r_j) = (r_j \ominus g_j) \oplus g_j$, where $\ominus$ and $\oplus$ denote the morphological erosion and dilation, respectively, and $g_j$ is the structuring element (SE) at the decomposition level $j$. With such a scheme, the signal $I$ is decomposed into a set of segments which reveal the shape information of the signal. Each half cycle of the current signal is decomposed into several fractions, the width of which is determined by the length of the corresponding SE. The height of these fractions can therefore be viewed as the increment of the current signal.

Prior to applying the decomposition scheme for inrush identification, the current $I$ is translated into two signals as

$$\begin{aligned} I' &= I + c_1 \\ I'' &= -I + c_2 \end{aligned} \tag{13}$$

Where $c_1$ and $c_2$ are predetermined constants, so that $I'$ and $I''$ are calculated by the morphological operators.

$I'$ is an input signal applied to deal with half cycles which contain the peaks of $I$, while $I''$ is the other input signal to process half cycles which contain the valleys of $I$. SEs $g_j$ are simple zero-valued flat lines with length of $l_j$. Assume that $f_r$ represents the sampling frequency of the system, then $l_j = j/f_r$ $(j = 1,2,\ldots,N/4)$, in which $N$ is the number of sampling points per cycle.

The process of the decomposition scheme is illustrated in Fig. 8. It can be seen from this figure that current $I'$ is the additional of $I$ and 20 A, and its mirror $I''$ is the additional of $-I$ and 50 A, which make $I' \geq 0$ and $I'' \geq 0$. The decomposition scheme beings from level 1 $(j = 1)$ and ends at level $j = N/4$. A group of components $s_j$ can be extracted from the currents $I'$ and $I''$ by using (12), and the height of the current increment for each component is measured and denoted as $I_j$. Assuming that the currents in Fig. 8 are sampled with 12 points per cycle, the decomposition scheme will iteratively run three times and six components of $s_j$, in total, are extracted from $I'$ and $I''$, respectively. $I_1$, $I_2$ and $I_3$ are the current increments of $s_j$, which are extracted from the current $I'$. Another group of current increments $I_1$, $I_2$ and $I_3$ are obtained from $I''$, respectively.

For identification magnetizing inrush current from other conditions by above approach a feature criterion can define to quantify the features of the current waveform, based on the measured current increments $I_j$ in comparison with the values calculated from a standard sinusoidal wave.

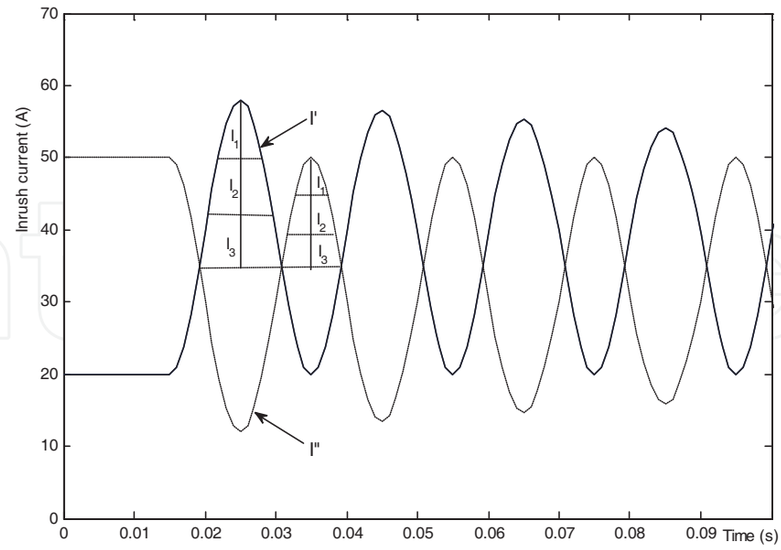


Fig. 8. Morphological decomposition of a current waveform

### 5.4 Neural network method for pattern recognition

Artificial Intelligence (AI) based techniques are well developed in the areas of pattern classification and recognition.

Neural networks (NNs) are composed of simple elements operating in parallel. These elements are inspired by biological nervous systems. As in nature, the connections between elements largely determine the network function. You can train a neural network to perform a particular function by adjusting the values of the connections (weights) between elements.

Typically, neural networks are adjusted, or trained, so that a particular input leads to a specific target output. The Fig. 9 illustrates such a situation. There, the network is adjusted, based on a comparison of the output and the target, until the network output matches the target. Typically, many such input/target pairs are needed to train a network.

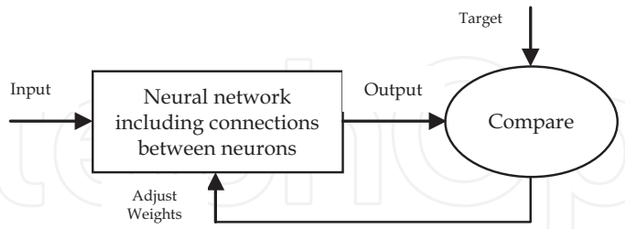


Fig. 9. Learning block diagram

Neural networks have been trained to perform complex functions in various fields, including pattern recognition, identification, classification, speech, vision, and control systems.

The NN applications were extended to variety of power system protective relaying and fault analysis problems.

The review indicates that most of the development efforts were related to the most common relaying functions such as distance protection for transmission lines and transformer current

differential protection. This is expected due to the importance, complexity and wide application of the mentioned protection principles. However, it is increasing to note that NN applications were mostly related to the fault detection and classification, which confirms the unique NN capability to act as a pattern classifier.

As per other non-relaying applications, it appears that fault analysis and detection of equipment incipient failure had created a lot of attention for NN applications. The ability of the NN architecture to process data in parallel and in a hierarchical fashion has been exploited in the fault analysis applications. The NN ability to learn from historical data was quite useful in the equipment diagnostic area. More developments are expected in both the fault analysis and equipment diagnostic areas.

Of the three most common types of ANNs, namely multi-layer, perceptron (MLP), Kohonen network (KN) and Hopfield network (HN), the MLP has hitherto been the mainstream of applications in power systems; this is principally because the supervised learning associated with the MLP is superior in terms of accuracy compared with either the KN or HN.

There are now widespread applications of ANNs in power systems. However, this part deals with only one problem, fault classification in double-circuit transmission lines using combined unsupervised/supervised in some detail (Aggarwal & Yonghua, 1998).

Parallel transmission lines which can significantly increase transmission capacity on existing systems are finding more widespread usage. However, there is difficulty in classifying the fault types on such lines using conventional techniques, principally because faulted phase(s) on one circuit have an effect on the phases of the healthy circuit due to mutual coupling between the two circuits. The problem is compounded by the fact that this coupling is highly non-linear in nature and is dependent on a complex interplay amongst a number of variables. As a consequence, the coupled phase(s) on the healthy circuit may sometimes be wrongly diagnosed as being faulted phase(s) under certain fault conditions. Thus conventional classifiers based on logical comparison techniques or linear algorithms are not well suited for such circuits. In this respect, neural computing has the very important attribute of being able to solve non-linear system identification problems through using neurons, links and learning algorithms, and hence ANNs are ideally suited to deal with complex non-linear fault classification problem.

ANNs have to be trained to learn and, in this respect, the training algorithms can be divided into supervised, unsupervised and combined unsupervised/supervised as shown in Fig. 10. Classifiers trained with supervision require data labels that specify the correct class during training. Clustering algorithms use unsupervised training and group unlabelled training data into internal clusters. Classifiers that use combined unsupervised/supervised training firstly use unsupervised training with unlabelled data to form internal clusters; labels are then assigned to clusters during the supervision stage. Different ANNs with, different training techniques have their own advantages and disadvantages. A typical supervised error back-propagation (EBP) network is a non-linear regression technique which attempts to minimise the global error. An EBP network can provide very compact distributed representations of complex data sets, and is smaller in size compared with a combined unsupervised/supervised ANN with the same inputs and outputs. However, training of an EBP network is very slow (time consuming), needs much larger training sets and it very easily gets stuck on local minima. Furthermore, it can be difficult to retrain the ANN with new training data.

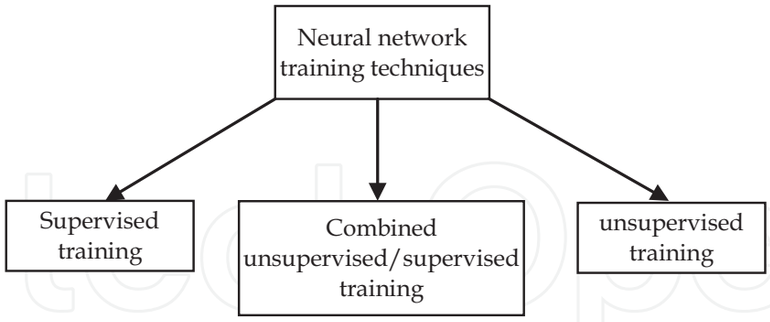


Fig. 10. ANN training techniques

Unsupervised learning means learning examples without teaching, i.e. there are no desired outputs. A typical unsupervised learning network is the KN. The network attempts to learn a topological map from an N-dimensional input space into a two dimensional feature space. Thus the network has many advantages over the EBP network, such as fast learning, a much smaller amount of training data etc. But, in view of the fact the network is without an output layer, it is not recommended to be used on its own for either pattern classification or other decision-making processes. Rather, it is used as the front end to an output layer with supervised learning and becomes a combined unsupervised/supervised (CUS) learning network, the subject of the technique described here.

This part proposes a fault type classification technique for double-circuit transmission lines using a CUS network.

The CUS-based classifier is a technique that separates object recognition into two parts: (i) feature extraction with unsupervised learning in the first stage, and (ii) classification with supervised learning sitting on the top, subsequently. An important basic principle is that the features must be independent of class membership, since the latter is not yet known at the feature extraction stage by definition. This implies that, if any learning methods are used for developing the feature extractors, they should be unsupervised in a sense, because the target class for each object is unknown. Fig. 11 typifies a CUS-based network.

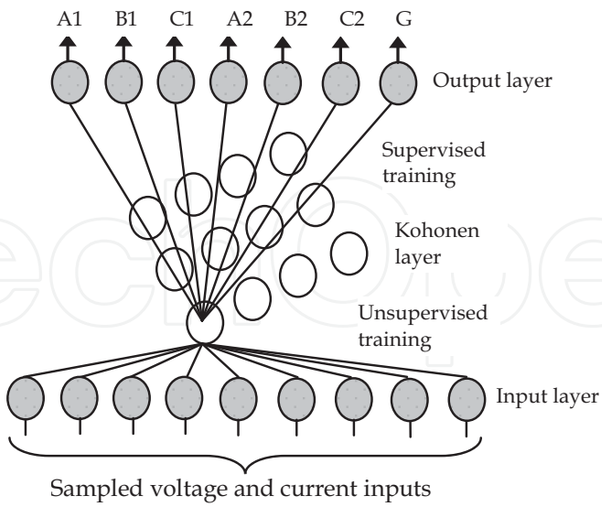


Fig. 11. CUS-based architecture network

The input vector for the CUS network comprises nine variables associated with the three voltage and six current signals in a double-circuit line. The feature extraction is based on time-domain windows, each window length being of three samples. The outputs are composed of seven variables Al, Bl, C1, PL2, B2, C2 and G; of these, '1' and '2' signify circuits 1 and 2, respectively, and variable G indicates whether ground is involved in a fault. As an example, if we get an output 1,0,0,0,0,0,1 this would indicate an 'a'-phase-earth fault on circuit 1.

In order to ascertain the attributes of the CUS network over a MLP network utilising a standard EBP training algorithm, a comparison in performance was made between the two ANNs. In this respect, the latter ANN also had nine variables but, unlike the CUS network, each window length used had four samples; a smaller window length made the convergence of the network to the requisite value extremely difficult. The hidden layer had 18 neurons and the output vector again comprised seven variables.

An extensive series of case studies showed that the MLP-based network converged after about 100 000 iterations (in approximately 45 minutes on a 133 MHz Pentium PC) and reached root-mean-square (RMS) error of 0.1. On the other hand, the CUS-based network converged after only 4000 iterations, i e in approximately 2 minutes, and reached a much lower RMS error of 0 03 Furthermore (although not shown here), of the 100 test cases considered, the misclassification rate was 6% and 1% for the MLP and CUS networks, respectively.

## 6. Wavelets and signal processing

### 6.1 Wavelet theory

Wavelet theory provides a unified framework for a number of techniques which had been developed independently for various signal processing applications. For example, multiresolution signal processing, used in computer vision; sub band coding, developed for speech and image compression; and wavelet series expansion, developed in applied

mathematics, have been recently recognized as different views of a signal theory. In fact, wavelet theory covers quite a large area. It treats both the continuous and the discrete-time cases. It provides very general techniques that can be applied to many tasks in signal processing, and therefore has numerous potential applications. In particular, the Wavelet Transform (WT) is of interest for the analysis of non-stationary signals, because it provides an alternative to the classical Short-Time Fourier Transform (STFT). In contrast to the STFT, which uses a single analysis window, the WT uses short windows at low frequencies. This is in the spirit of constant relative bandwidth frequency analysis. The WT is also related to time-frequency analysis.

### 6.2 Signal Construction Using Wavelets

Wavelet theory establishes that a general transient signal can be constructed by the superposition of a set of special signals (different structures occurring at different time scales and at different times). These special signals may be selected as wavelets. For a set of wavelets to be admissible as a basic building block, they must satisfy two basic conditions: they must be oscillatory, and they must decay to zero quickly. If these conditions are combined with the condition that the wavelets must also integrate to zero, then these conditions are the non-rigorous admissibility criteria that must be satisfied to be a wavelet.

The selection of the best wavelets is a function of the characteristics of the signal to be processed. For example, a musical tone can be described by four basic parameters: intensity, frequency, time duration, and time position. Thus, the key to the process is to select a wavelet to realize the signal in terms of the best basis and most efficient superposition. The best and most efficient wavelet set is also a function of the objective of the reconstruction. Typical applications are compactation for storage purposes, fast reconstruction for signal identification, and efficient reconstruction for signals analysis. The selection of the best wavelet basis is a function of the characteristics of the original signal to be reconstructed or analyzed. It also depends on the compact support and/or fast reconstruction required by the process.

For image processing, for example, and due to improved resolution and efficiencies, the best wavelet basis is usually found to be in a family of multiresolution functions that are orthogonal or biorthogonal. However, these bases exploit (for efficiency reasons) a specialized spacing in the wavelet parameters that specify position (shift) and dilation (width) which requires the scale and translation parameters to be spaced by integer powers of 2. The spacing that is usually used is called a dyadic lattice. The nature of power system signals seems to point towards trigonometric based wavelets. For power system electromagnetic transient signals, the wavelet basis should have two desirable characteristics:

1. Reduce the number of wavelet components that describe the signals
2. Reveal the natural (physical) transient oscillatory components of the signal.

### 6.3 Differential protection based on wavelet transform

Traditional digital protective relays present several drawbacks; for instance, they are usually based on algorithms that estimate the fundamental component of the current and voltage signals neglecting higher frequency transient components. Moreover, phasor estimation requires a sliding-window of a cycle that may cause a significant delay. Furthermore,

accuracy is not assured. The Fourier transform is a very useful tool for analyzing the frequency content of stationary processes. When dealing with non-stationary processes, however, other methods for determining the frequency content must be applied.
For this reason wavelet decomposition is ideal for studying transient signals and obtaining a much better current characterization and a more reliable discrimination. Wavelets allow the decomposition of a signal into different levels of resolution (frequency octaves). The basis function (Mother Wavelet) is dilated at low frequencies and compressed at high frequencies, so that large windows are used to obtain the low frequency components of the signal, while small windows reflect discontinuities.
Wavelet transform has a special feature of variable time-frequency localization which is very different from windowed Fourier transform.
Differential protection algorithms based on FFT have disadvantages including the neglecting of high frequency harmonics. Furthermore, different windowing techniques should be applied to calculate the current and voltage phasors and this causes significant time delay for the protection relay. In this case, accuracy is not assured completely. Due to increased standards of the delivered energy quality such as IEEE 519, high performance algorithms should be taken into account.
The Grossmann & Morlet (1984) definition of the continuous wavelet transform (CWT) for a 1-D signal $f(x) \in L^2(R)$ is:

$$W(a,b) = k(a) \int_{-\infty}^{+\infty} f(x)\overline{\Psi}\left(\frac{b-x}{a}\right) dx$$
$$= k(a) \int_{-\infty}^{+\infty} f(x)\widetilde{\Psi}\left(\frac{x-b}{a}\right) dx \quad (14)$$

Where $\widetilde{\Psi}(x) = \overline{\Psi}(x)$; $a \in R^+$ and $b \in R$, are the scale and the position parameters, respectively, with $R^+$ being the set of positive real numbers; $L^2(R)$ denotes the Hilbert space of square integrable functions, and the bar denotes the conjugated complex. The constant $k(a)$ can be taken to be $1/\sqrt{a}$ in order to insure normalization in energy of the set of wavelets $\Psi(\frac{x-b}{a})$ obtained by a translation and dilation of the "mother wavelet" $\Psi$. The first formula permits the interpretation of the wavelet transform as a convolution product; the second as a correlation function. If the wavelet is symmetric and real $\widetilde{\Psi} = \overline{\Psi}$ (as in the case of the Poission wavelet) both notions coincide (Moreau et al. 1997).
The main advantage of the CWT is that it reveals the signal content in far greater detail than either Fourier analysis or the discrete wavelet transform (DWT). The continuous nature of the wavelet function is kept up to the point of sampling the scale-translation grid used to represent the wavelet transform is independent of the sampling of the signal under analysis.
In this case, the discrete wavelet transform is:

$$\widetilde{W}_{l,k} = \int_{-\infty}^{+\infty} f(x)\Psi_{l,k}(x)dx \quad (15)$$

and the inverse discrete transform (IDWT) is

$$f(x) = \sum_{l=-\infty}^{\infty} \sum_{k=-\infty}^{\infty} \widetilde{W}_{l,k} \ \Psi_{l,k}(x) \tag{16}$$

In the $L^2$ sense.

The advantage of analysing a signal with wavelets is that it enables one to study the local features of the signal with a detail matched to their characteristic scale. In the temporal domain such a property allows for an effective representation of transient signals. We can say that the DWT enables one to make a multiresolution analysis of a signal. It is possible to have both smooth wavelets with compact support and symmetry of the associated scaling functions and this avoids bias for the locations of maxima and minima of the signal.

The Wavelet Transform is well suited to the problem in this study. It is similar to the Fourier transform, but uses a basis function that decays rapidly from a central feature rather than the infinite sine function. For this reason wavelet decomposition is ideal for studying transient signals and obtaining a much better current characterization and a more reliable discrimination.

The application areas of wavelets cover time and frequency analysis, electromagnetic analysis, filters, integral equations, transient analysis, picture processing, and data compressing techniques.

In Figure 12, time and frequency localization are shown for the short time fast Fourier Transform. This approach was presented by Gabor in 1945.

In Figure 13, time and frequency localization are shown for the continuous wavelet transform. This approach was presented by Morlet in 1980.

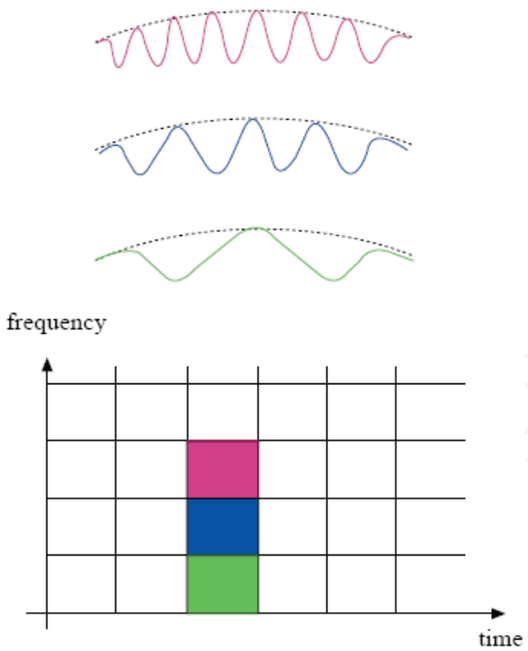


Fig. 12. Gabor localizes the short time fast Fourier Transform (STFFT) in 1945

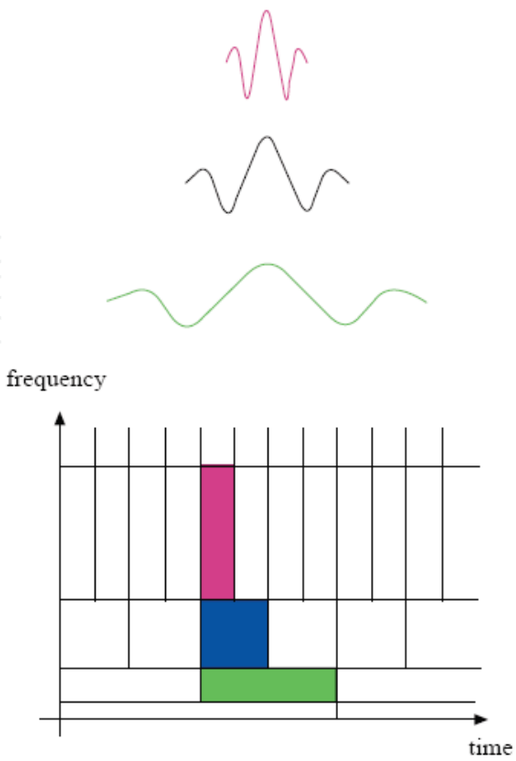


Fig. 13. Morlet proposes the continuous wavelet transform in 1980

### 6.4. Identification of signals using wavelet transform

A wavelet-based signal processing technique is an effective tool for power system transient analysis and feature extraction. An application of wavelet analysis to identify various types of currents flowing through a power transformer.

Recently, several new protective schemes have been proposed to deal with problem in power transformer protection based on wavelet transforms (WT). Some of wavelet based methods use voltage and current signals for identification magnetizing inrush current from internal fault currents. The drawback of these methods is that those require the measurement of voltage in addition to current that increases the cost of hardware implementation. Another methods use combination of WT and neural network. Generally, in these methods a WT use as a pre-processor and the output of the wavelet is the input of the artificial neural network. The required algorithm training is some drawbacks of these algorithms.

This work proposes a new algorithm based on the Wavelet Transform (WT) to identify magnetizing inrush current from internal fault current in three phase power transformers. To discriminate between various cases, the developed method uses different features of fault and inrush currents. At first the wavelet transform technique is applied to decompose transformer differential currents into approximated and detailed wavelet components (i.e. An and D1 – Dn). Each of these levels are time domain signals cover specific frequency band. Then, a diagnosis criterion by using the specific wavelet coefficients is defined. This criterion discriminate internal faults from inrush currents accurately and in short time (less than

5 ms) after the disturbance. The proposed algorithm is evaluated using various simulated different inrush and internal fault current signals on a power transformer. Magnetizing inrush currents and fault currents has been developed using the ATP-EMPT software. Then using wavelet and defined criteria, the transient fault current and magnetizing inrush current are differentiated. The results proved that the proposed technique is able to offer the desired responses and could be used as a very fast and accurate method.

### 6.4.1 proposed algorithm

The new proposed algorithm is based on waveform analysis of the fault and inrush currents. Fig. 14 shows the features of these waveforms. As is shown, the inrush current has a non-sinusoidal shape and there is a dead period per cycle in magnetizing inrush during which the current will be near zero because of the saturation characteristic of the transformer. Magnetizing inrush also exhibit a characteristic peaked wave which is caused by asymmetric saturation of the transformer core. The inrush current at the switching time increases very slowly and is near zero; while the progress of slope variation is increasing and after a few samples it amplifies in rapidly. However, when a fault occurs, slope of the differential current at the fault time is high, and slope variation decrease as time passes. These different behaviors could be used for discrimination of various cases.

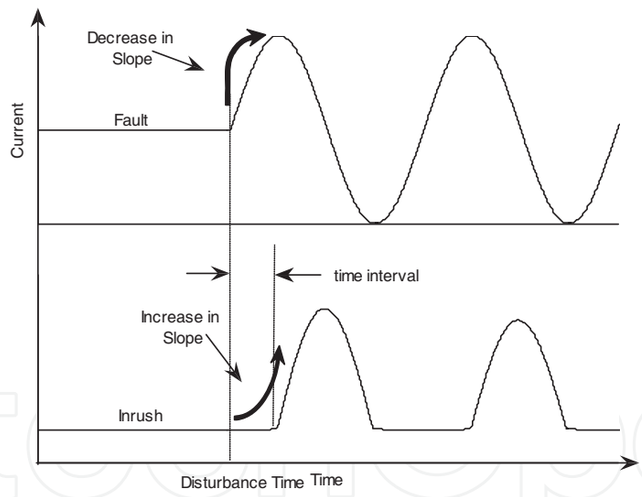


Fig. 14. Features of fault and inrush waveforms

The proposed algorithm is based on this fact that the location of rapid slope variation, for inrush current occurs after internal fault by a time interval. A large slope in the time domain means that there are higher frequencies in the frequency domain. Therefore, following the internal fault, the amplitude of the high frequencies at the initial instants has larger values than the other times. However, following the inrush current the amplitude of the high frequencies components at the initial instants is lower than the other times. The differential current and resultant frequency levels (A7 and D1-D7) from WT due to inrush current and AB-G internal fault at t=0.1 s are shown in Figs. 15 and 12 respectively.

Through various simulations, it is found that the mentioned features appear in D4 wavelet (Table 2). The time duration between the time of disturbance and the maximum peak of the differential current in D4 is considered as the diagnosis criterion, and called $t_p$.

| Wavelet Coefficients | Frequency band (Hz) |
|---|---|
| A7 | 0-39.06 |
| D7 | 39.06-78.125 |
| D6 | 78.125-156.25 |
| D5 | 156.25-312.5 |
| D4 | 312.5-625 |
| D3 | 625-1250 |
| D2 | 1250-2500 |
| D1 | 2500-5000 |

Table 2. Wavelet frequency levels for sample rate 10 khz

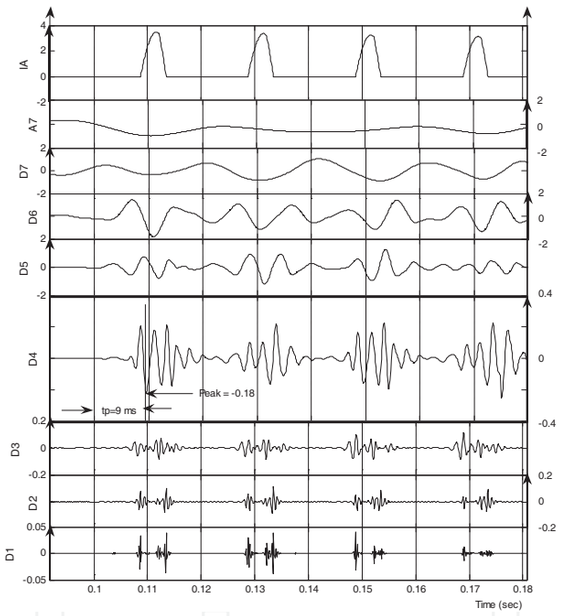


Fig. 15. Differential current and related frequency levels, inrush

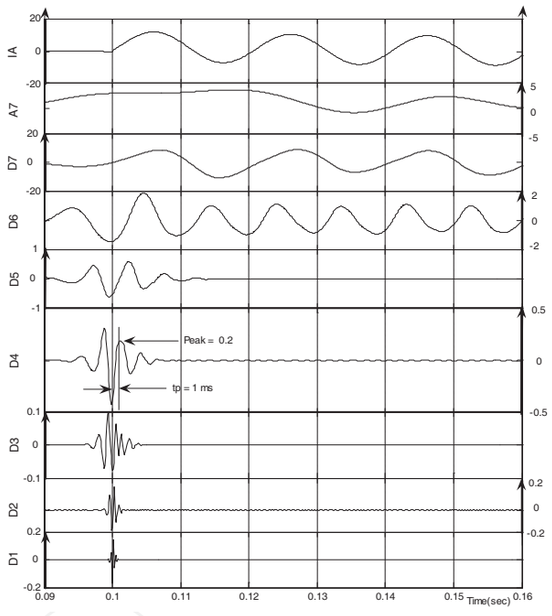


Fig. 16. Differential current and related frequency levels, AB-G fault

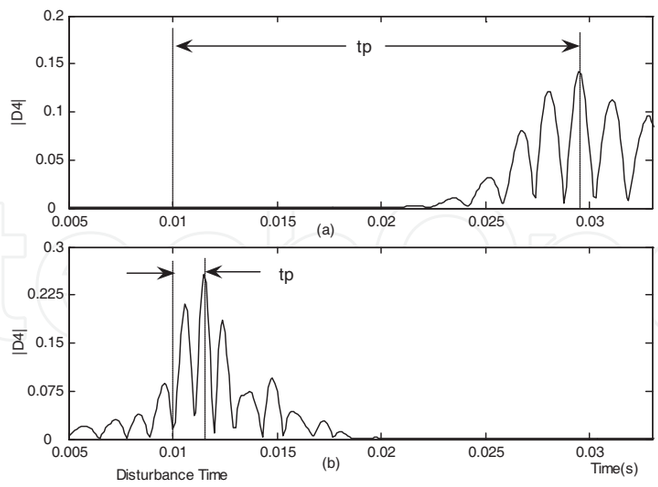


Fig. 16. D4 and $t_p$ for (a) inrush (b) internal fault

Fig. 16 shows the interval time $t_p$ and the absolute values of the differential current waveforms for the fault current and inrush current at frequency level D4. In the case of inrush current, $t_p$ is higher than a setting $\left(t_p > t_{setting}\right)$, and in the case of internal fault, $t_p$ is lower than a setting $\left(t_p < t_{setting}\right)$. Comparison of $t_p$ with $t_{setting}$ is considered for three phases and if at least in one phase $t_p < t_{setting}$, a fault is occurred and the trip command is issued and else, there is no any trip command. As shown in Fig. 16, the above criterion can be used to discriminate the internal fault from the inrush current in about a quarter a cycle. It provides a very quick and simple algorithm.

The performance of the proposed algorithm was evaluated for different types of fault and inrush currents. Different cases of fault currents are simulated where some factors affecting the characteristics of the current, such as type of fault and load condition are considered. Different cases of inrush current are also simulated by varying some parameters that influence the characteristics of this current (e.g. residual core flux and voltage angle). Moreover, different cases for simultaneous inrush and fault conditions are simulated.

**A) Inrush Current**

For the case of magnetizing inrush current, the no-load transformer at a supply line voltage of 400 kV is considered. Fig. 17 shows the three-phase differential currents and the frequency range D4 for $I_{diff-a}$, $I_{diff-b}$ and $I_{diff-c}$. Switching time is $115\ ms$ and residual core flux and phase angle of the supply is chosen $B_{rA} = 50\%$ and $\theta_A = 0^{\circ}$ respectively. In this figure the frequency range D4 and relevant differential current (doted curve) in each phase are shown after initiation of disturbance. As it is seen from the Fig. 18 $t_{p-a} = 4.6\ ms$, $t_{p-b} = 4.6\ ms$ and $t_{p-c} = 6.4\ ms$ are obtained.

Investigation of various simulations reveals that values of $t_p$ for various inrush currents are usually greater than $4 - 5\ ms$ (i.e., at least there is a period that for it $t_p$ is greater than this range). Also for internal fault currents there is a period that for it $t_p$ is less than $0.5 - 1.5\ ms$. Therefore we can choose $t_{setting}$ equal to $2 - 3\ ms$. In this paper $t_{setting}$ is chosen as $2\ ms$. As seen from Fig. 18 $t_{p-a} > t_{setting}$, $t_{p-b} > t_{setting}$ and $t_{p-c} > t_{setting}$ which shows

that there is no fault and the maltrip is not issued. Obtained results for different conditions of inrush currents are shown in Table 3. This table shows the value of $t_p$ for different phases due to different inrush current. The first column shows phase a voltage angle at the instant of switching. In the second column differential current of various phase are shown. In both no-load and full-load cases shown in next columns, influence of remnant fluxes in the power transformer core at instant of switching as percent of the rated flux have been studied.
As shown in this table for all of the studied cases, the obtained value of $t_p$ is greater than 2 $ms$. As a result all of these cases are correctly classified as inrush cases.

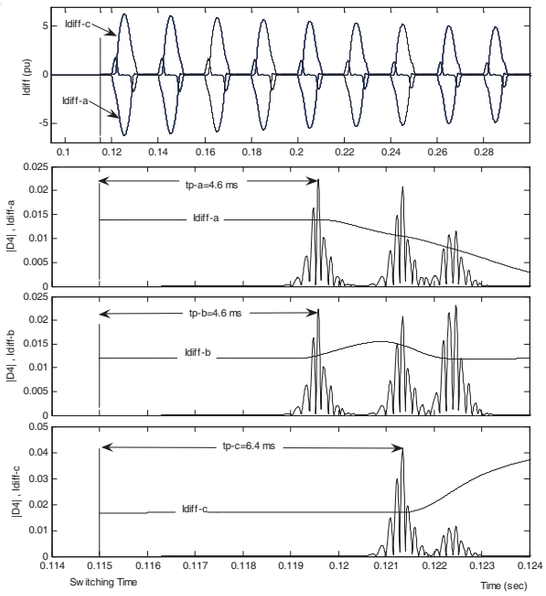


Fig. 18. Frequency range |D4| for $I_{diff-a}$, $I_{diff-b}$ and $I_{diff-c}$ for unloaded magnetizing inrush

| $\theta_A$ | Phase | No load | | Full load | |
|---|---|---|---|---|---|
| | | $B_{rA}=0$ $B_{rB}=0$ $B_{rC}=0$ | $B_{rA}=58\%$ $B_{rB}=0$ $B_{rC}=-58\%$ | $B_{rA}=0$ $B_{rB}=0$ $B_{rC}=0$ | $B_{rA}=58\%$ $B_{rB}=0$ $B_{rC}=-58\%$ |
| 0 | A | 5.3 | 6.1 | 5.2 | 4.8 |
| | B | 4.8 | 6 | 4.8 | 4.8 |
| | C | 4.8 | 5.2 | 4.8 | 6.1 |
| 80 | A | 4.7 | 6.8 | 4.8 | 3 |
| | B | 4.6 | 6.8 | 4.7 | 6.2 |
| | C | 6.1 | 6.8 | 5.3 | 3.8 |
| 120 | A | 4.8 | 5.2 | 4.8 | 4.8 |
| | B | 5.3 | 6.1 | 5.2 | 4.8 |
| | C | 4.8 | 6 | 4.8 | 4.8 |

Table 3. Values of $t_p$ (ms) for inrush currents

**B) Fault Current**

To obtain the simulation data for internal fault, different faults such as single line-to-ground fault, line-to-line fault, line-to-line-to-ground fault and three phase fault simulated on the inside of the transformer zone with a balanced Y-connected load of phase connected to the secondary side. The resistance at the fault location is chosen as zero and transformer is assumed to have rated load (in the case of on-load simulations).

Fig. 19 shows three-phase differential currents and the frequency range D4 due to $I_{diff-a}$, $I_{diff-b}$ and $I_{diff-c}$. In this case, the line-to-line-to-ground fault (fault AB-G) on the secondary side of the transformer is occurred, the transformer is full-load and the fault time is $20$ ms. As it is seen from the Fig. 19 the time duration between of the initiate instant of disturbance (fault time= 20 ms) to the maximum peak of the differential current in D4, for each phases are computed as: $t_{p-a} = 0.5$ ms, $t_{p-b} = 0.5$ ms and $t_{p-c} = 2.2$ ms. These values in each phase will be compared with $t_{setting}$. As seen Fig. 19 $t_p$ for phase a and phase b are lesser than $t_{setting}$ ($t_{p-a} < t_{setting}$, $t_{p-b} < t_{setting}$ and $t_{p-c} > t_{setting}$) which shows the disturbance is a fault. Respect to obtained results it is founded that the proposed method discriminate fault from inrush current quickly, less than a quarter a cycle after the disturbance.

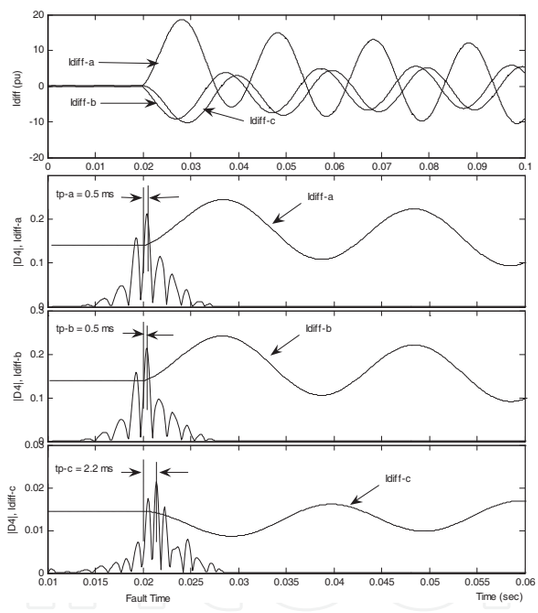


Fig. 19. Frequency range |D4| for $I_{diff-a}$, $I_{diff-b}$ and $I_{diff-c}$ for AB-G internal fault

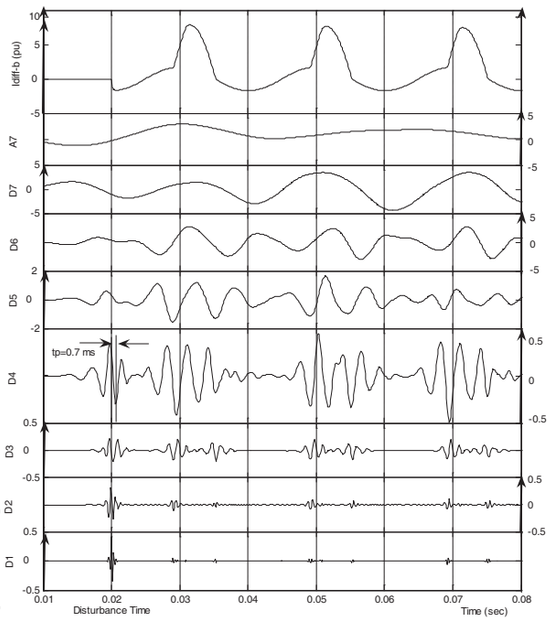


Fig. 20. Differential current and related frequency levels for simultaneous internal fault AB-G and inrush

The results of application of the proposed algorithm for internal fault conditions have been summarized in Table 4. Simulations have been carried out for different faults in no-load and on-load of power system.

**C) Simultaneous Internal Fault and Inrush Current**

After studying fault and inrush currents cases separately, some more complicated cases, i.e. simultaneous internal fault and inrush current are considered. In Table 5, four different cases have been studied and in all cases the fault has been properly diagnosed fast and reliably. Fig. 20 shows the differential current (phase B) for simultaneous inrush and fault (AB-G) on the primary side at $t = 0.02$ s as well as WT coefficients in D1-D7 and A7. Fig. 21 shows the three phase differential currents and D4 for $I_{diff-a}$, $I_{diff-b}$ and $I_{diff-c}$. As it is seen from the Fig. 21 the $t_p$ amount for differential current in D4 for three phases, is $t_{p-a} = 0.07$ ms, $t_{p-b} = 0.07$ ms and $t_{p-c} = 4.8$ ms. As seen Fig. 21 $t_p$ for phase a and phase b are less than $t_{setting}$ ($t_{p-a} < t_{setting}$, $t_{p-b} < t_{setting}$ and $t_{p-c} > t_{setting}$). Thus, the occurrence of the fault is detected accurately shorter than a quarter of a cycle ($t_{setting} = 2$ ms).

| $\theta_1$ | phase | No load | | | | Full load | | | |
|---|---|---|---|---|---|---|---|---|---|
| | | a-g | a-b | a-b-g | a-b-c | a-g | a-b | a-b-g | a-b-c |
| 0 | a | 0.1 | 0.1 | 0.1 | 0.1 | 0.1 | 0.1 | 0.1 | 0.1 |
| | b | 0.7 | 0.1 | 0.1 | 1.5 | 0.7 | 0.12 | 0.1 | 1.5 |
| | c | 0.1 | 0.1 | 0.1 | 0.1 | 0.1 | 0.1 | 0.12 | 0.11 |
| 80 | a | 0.1 | 0.13 | 0.1 | 0.1 | 0.12 | 0.1 | 0.1 | 0.1 |
| | b | 4.8 | 0.11 | 0.1 | 0.1 | 5 | 0.13 | 0.1 | 0.11 |
| | c | 0.1 | 0.1 | 1.5 | 0.1 | 0.11 | 0.1 | 1.5 | 0.1 |
| 120 | a | 0.1 | 0.1 | 0.1 | 0.1 | 0.1 | 0.1 | 0.1 | 0.1 |
| | b | 1.5 | 0.1 | 0.1 | 0.1 | 3.1 | 0.1 | 0.1 | 0.1 |
| | c | 0.1 | 0.1 | 0.1 | 1.5 | 0.1 | 0.1 | 0.1 | 1.5 |

Table 4. Values of $t_p$ $(ms)$ for internal faults

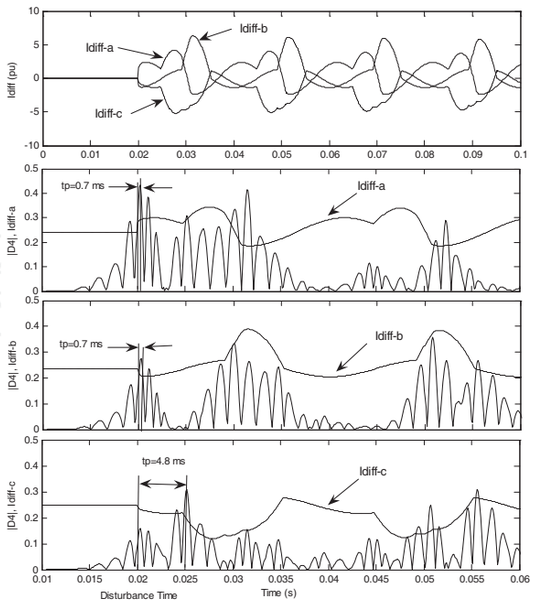


Fig. 21. Differential currents and |D4| for three phases for simultaneous internal fault AB-G and inrush current

| $\theta_A$ (DEG.) | $B_r$ | PH ASE | NO LOAD | | | | FULL LOAD | | | |
|---|---|---|---|---|---|---|---|---|---|---|
| | | | A-G | A-B | A-B-G | A-B-C | A-G | A-B | A-B-G | A-B-C |
| 80 | $B_{rA}=0$ $B_{rB}=0$ $B_{rC}=0$ | A | 0.2 | 0.1 | 0.1 | 2.5 | 0.1 | 0.1 | 1.5 | 1.5 |
| | | B | 0.1 | 0.2 | 0.1 | 0.1 | 0.1 | 0.2 | 0.1 | 0.1 |
| | | C | 5.1 | 0.1 | 2.5 | 0.1 | 4.6 | 0.1 | 0.1 | 0.1 |
| | $B_{rA}=58\%$ $B_{rB}=0$ $B_{rC}$ =-58% | A | 0.2 | 0.1 | 2.5 | 0.2 | 0.1 | 0.2 | 0.1 | 0.1 |
| | | B | 0.2 | 0.1 | 0.1 | 0.2 | 3.5 | 0.2 | 1.5 | 0.1 |
| | | C | 4.6 | 0.1 | 0.1 | 0.1 | 0.1 | 0.1 | 0.1 | 0.1 |

Table 5. Values of $T_P$ (ms) for simultaneous inrush currents and internal faults

## 7. Conclusion

This manuscript invetigates the coomon approachs for pattern recognition of current signals for identification of differential currets which flow into the differential relays. Final it presents a successful technique to distinguishing between internal faults and inrush currents in power transformers using wavelet transform. The diagnosis process in this method is based on the different characteristics of differential currents waveforms. A diagnosis criterion by quantifying the extracted features is defined in terms of time difference of amplitude of wavelet coefficients over a specific frequency band. By using this criterion function for three phases, internal faults can be accurately discriminated from inrush current. Several cases are used for testing the proposed algorithm. The simulation results show fast, accurate and reliable capabilities of the algorithm to identify different types of currents flowing in a power transformer under various inrush currents and internal faults conditions. The proposed scheme is a powerful yet simple way of assigning transformer differential current to inrush and fault groups.

## 8. References

ABB Company (2003). Technical Reference Manual Of RET 521*2.5-Transformer Protection Terminal, ABB Company, 1MRK 504 036-UEN, December 2003.

Aggarwal and Yonghua Song (1998). Artificial neural networks in power systems, power engineering journal december 1998.

A. Guzman, S. Zocholl, G. Benmouyal, and H. J. Altuve (2001). A currentbased solution for transformer differential protection__part I: Problem statement, IEEE Trans. Power Del., vol. 16, no. 5, pp. 485–491, Oct. 2001.

A. Guzman, S. Zocholl, G. Benmouyal, and H. J. Altuve (2002). A current-based solution for transformer differential protection__part II: Relay description and evaluation, IEEE Trans. Power Del., vol. 17, no. 5, pp. 886–893, Oct. 2002.

A. Rahmati, and M. Sanaye-Pasand (2008). New Method for Discrimination of Transformers Internal Faults from Magnetizing Inrush Currents Using Wavelet Transform, IEEE POWERCON2008 Conference, New Delhi, India, 12-15 October 2008.

H. Mortazavi and H. Khorashadi-Zadeh (2004). A new inrush restraint algorithm for transformer differential relay using wavelet transform, in Proc. Int. Conf. Power System Technology-Powercon, Singapore, Nov. 21–24, 2004, pp. 1705–1709.

M.R. Zaman and M.A. Rahman (1998). Experimental testing of the artificial neural network based protection of power transformers, IEEE Trans. Power Del., vol. 13, no. 2, pp. 510-517, Apr. 1998.

Omar A. S. Youssef (2003). A wavelet-based technique for discrimination between faults and magnetizing inrush currents in transformers, IEEE Trans. Power Del., vol. 18, no. 1, pp. 170–176, Jan. 2003.

P. L. Moa and R. K. Aggarwal (2001). A novel approach to the classification of the transient phenomena in power transformer using combined wavelet transform and neural network, IEEE Trans. Power Del. ,vol. 16, no. 4, pp. 654-660, Oct. 2001.

S. A. Saleh and M. A. Rahman (2005). Modeling and Protection of a Three-Phase Power Transformer Using Wavelet Packet Transform, IEEE TRANSACTIONS ON POWER DELIVERY, VOL. 20, NO. 2, APRIL 2005.

S.Sudha and A. Ebenezer Jeyakumar (2007). Wavelet and ANN Based Relaying for Power Transformer Protection, Journal of Computer Science 3 (6): 454-460, 2007, ISSN 1549-3636.

Y. Sheng and M. Steven (2002). Decision trees and wavelet analysis for power transformer protection, IEEE Trans. Power Del., vol. 17, no. 2, pp. 429–433, Apr. 2002.

Z. Lu, W. H. Tang, T. Y. Ji and Q. H. Wu (2009). A morphological scheme for inrush identification in transformers protection, IEEE Trans. Power Del., Vol. 24, no. 2, pp. 560-568, April 2009


**Pattern Recognition**
Edited by Peng-Yeng Yin

ISBN 978-953-307-014-8
Hard cover, 568 pages
**Publisher** InTech
**Published online** 01, October, 2009
**Published in print edition** October, 2009

For more than 40 years, pattern recognition approaches are continuingly improving and have been used in an increasing number of areas with great success. This book discloses recent advances and new ideas in approaches and applications for pattern recognition. The 30 chapters selected in this book cover the major topics in pattern recognition. These chapters propose state-of-the-art approaches and cutting-edge research results. I could not thank enough to the contributions of the authors. This book would not have been possible without their support.



**InTech Europe**
University Campus STeP Ri
Slavka Krautzeka 83/A
51000 Rijeka, Croatia
Phone: +385 (51) 770 447
Fax: +385 (51) 686 166
www.intechopen.com

**InTech China**
Unit 405, Office Block, Hotel Equatorial Shanghai
No.65, Yan An Road (West), Shanghai, 200040, China
中国上海市延安西路65号上海国际贵都大饭店办公楼405单元
Phone: +86-21-62489820
Fax: +86-21-62489821

IntechOpen